Comparative Study between SPWM and SVPWM control of a three level voltage inverter dedicated to a variable speed wind turbine

Belkacem Belkacem, Abdelhakem-Koridak Lahouari, Rahli Mostefa

Electrical Engineering Faculty, Electrical Department, University of Science and Technology Mohamed Boudiaf of Oran—Algeria. Laboratory (LORE),B.P 1505 El Mnaouer USTMB-Oran-Algeria Tel & Fax: 00.213-41-62 71 63

Abstract

In this paper, a power production system containing a variable speed wind turbine equipped with a Doubly Fed Induction Generator (DFIG) is presented, the DFIG stator is connected directly to the grid, and the rotor is connected by a three level three phase inverter with a Neutral Point Clamping structure (NPC). This last must be then dimensioned to forward only the available power of the rotor. In this work, a comparative study of two command strategies of the inverter is detailed, by separate order control: Firstly Sinus Pulse Width Modulation (SPWM) and secondly Sinus Vectorial Pulse Width Modulation (SVPWM). All the simulation models are built in MA TLAB/Simulink software and the performance of the control system is evaluated through FFT analysis of results.

Keywords: DFIG, SPWM, SVPWM, FFT, THD analysis, three levels inverter

1. Introduction

Concerns about climate change and air pollution have attracted great interest in technologies for the generation of clean and green renewable energy. Among the various renewable energy sources, wind energy has contributed greatly due to its ready availability and economical aspect. The total installed capacity of wind generation has been continuously increasing over the last fifteen years [1]. Wind energy systems are among the most successful technologies, not only in technical terms but also in the industrial field. Power converters have developed a significant role in the integration of wind power into the electrical grid [2]. Power converters allow for variable speed operation of wind turbines and enhanced power extraction [3]. The use of power electronics components has resulted in the creation of extra degrees of freedom, thereby making it possible to implement more complex control algorithms and optimize wind turbine performances [4].

The variable speed wind turbine equipped with doubly fed induction generator (DFIG) has gained popularity due to the development in modern power electronics. DFIG has many advantages, including variable speed constant frequency operation, independent active and reactive power control, reduced flicker, low cost converters and reduced power losses [5]. DFIG is basically a system consisting of a wound rotor generator and stator windings directly connected to a three phase grid. The rotor windings are fed by a variable frequency converter (VFC). Hence the cost of converters has been reduced greatly.

The wind turbine is modeled to find a relationship between electromagnetic torque and mechanical wind speed. Section III describes the mechanical and electrical model of the DFIG. Two control strategies of the three level inverter are given in section IV. Finally, the simulation and results are presented; performances are then evaluated taking into account the Fast Fourier Transform (FFT) and THD analysis.

2. Wind turbine model

Mechanical power available on the shaft of a wind turbine is expressed by [6]:

$$P_v = \frac{1}{2}\rho S v_v^3 = \frac{1}{2}\rho\pi R^2 v_v^3 \qquad (1)$$

where: ρ—air density (1.25 kg/m^3); R—blade length in meters; v_v— wind velocity in m/s.

The aerodynamic power extracted from the wind turbine can be calculated as:

$$P_{Turb} = C_p P_v = \frac{1}{2}\rho S v_v^3 = \frac{1}{2}\rho\pi R^2 v_v^3 \cdot C_p(\lambda,\beta) \qquad (2)$$

*Corresponding author

Email address: `belkacem.belkacem@univ-usto.dz` (Belkacem Belkacem)

$$\lambda = \frac{\Omega_{Turb} \cdot R}{v_v} \quad (3)$$

where: C_p—power coefficient; β—pitch angle (deg); λ— tip speed ratio; Ω_{Turb}—turbine speed, rd/s.

No wind turbine could convert more than 59% of the kinetic energy of the wind into mechanical energy turning a rotor [7]. This is known as the Betz limit, and it is the theoretical maximum coefficient of power for any wind turbine: $C_p$max = 16/27≈0.593.

The multiplier is mathematically modeled by the following equations:

$$\begin{cases} T_m = \frac{T_{turb}}{G} \\ \Omega_{Turb} = \frac{\Omega_m}{G} \\ J_T = \frac{J_{Turb}}{G^2} + J_g \\ T_{Turb} = \frac{P_{Turb}}{\Omega_{Turb}} \end{cases} \quad (4)$$

where: Ω_{turn} et Ω_m—turbine speed respectively before and after the multiplier; T_{turb}—aerodynamic torque; T_m— torque after the multiplier; G—gear ratio; J_g— generator inertia; J_T—total inertia; J_{Turb}— turbine inertia.

The fundamental equation of dynamics to determine the evolution of the mechanical speed from the total mechanical torque (T_{mec}) applied to the rotor:

$$J_T \frac{d\Omega_{mec}}{dt} = T_{mec} = T_m - T_{em} - C_f\Omega_{mec} \quad (5)$$

where: T_{em}— electromagnetic torque; C_f—viscous friction coefficient.

3. Modeling of the DFIG

The d-q axis representation of DFIG is used for modeling, considering flux as variable based on Park's model. All rotor quantities are referred to the stator side. The d^s–q^s notation corresponds to the stator side axes and $d^r - q^r$ corresponds to the rotor side axes. The DFIG model represented by voltage equations (6), where w_s is the rotational speed of the synchronous reference frame, w_r. The stator and rotor side flux linkage equations are given as [5, 6, 8]:

$$\begin{aligned} V_{sd} &= R_sI_{sd} + \frac{d\Phi_{sd}}{dt} - \omega_s\Phi_{sq} \\ V_{sq} &= R_sI_{sq} + \frac{d\Phi_{sq}}{dt} + \omega_s\Phi_{sd} \\ V_{rd} &= R_rI_{rd} + \frac{d\Phi_{rd}}{dt} - (\omega_s - \omega_r)\Phi_{rq} \\ V_{rq} &= R_rI_{rq} + \frac{d\Phi_{rq}}{dt} + (\omega_s - \omega_r)\Phi_{rd} \end{aligned} \quad (6)$$

The stator and rotor flux can be expressed as:

$$\begin{aligned} \Phi_{sd} &= L_sI_{sd} + L_mI_{rd} \\ \Phi_{sq} &= L_sI_{sq} + L_mI_{rq} \\ \Phi_{rd} &= L_rI_{rd} + L_mI_{sd} \\ \Phi_{rq} &= L_rI_{rq} + L_mI_{sq} \end{aligned} \quad (7)$$

Electromagnetic torque is also expressed in terms of currents and flux:

$$C_{em} = p\frac{L_m}{L_s}(\Phi_{sd}I_{qr} - \Phi_{sq}I_{dr}) \quad (8)$$

where: R_s, R_r—are respectively the stator and rotor resistances; L_s, L_r— inductances of the stator and rotor windings;
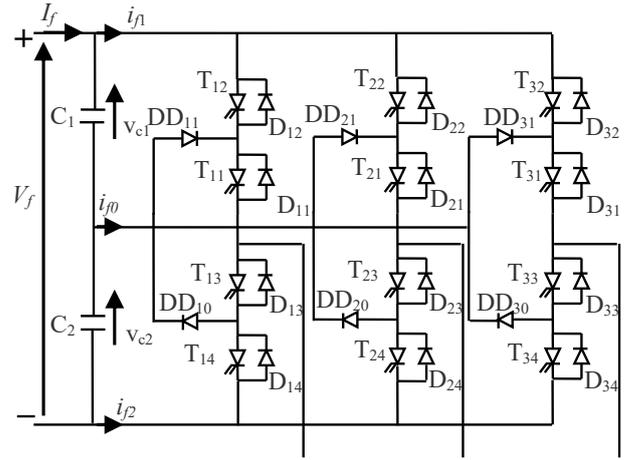

Figure 1: Three level inverter structure

L_m— is the mutual inductance; V_{ds}, V_{qs}, V_{dr} et V_{qr}—direct and quadrate components of the space phasors of the stator and rotor voltages; I_{ds}, I_{qs}, I_{dr} and I_{qr}—direct and quadrate components of the space phasors of the stator and rotor currents; φ_{ds}, φ_{qs}, φ_{dr} and φ_{qr}—direct and quadrate components of the space phasors of the stator and rotor flux respectively; ω_s—rotational speed of the synchronous reference frame; ω_r—rotor speed

p—number of pair poles.

Active and reactive powers at the stator (P_s, Q_s), and the rotor (P_r, Q_r) are defined as:

$$\begin{cases} P_s = V_{sd}I_{sd} + V_{sq}I_{sq} \\ Q_s = V_{sq}I_{sd} - V_{sd}I_{sq} \\ P_r = V_{dr}I_{dr} + V_{qr}I_{qr} \\ Q_r = V_{qr}I_{dr} - V_{dr}I_{qr} \end{cases} \quad (9)$$

4. Three level voltage inverter theory

4.1. Structure of the three level inverter

The three level inverter [8, 9] is composed of three arms and two dc voltage sources. Each inverter arm consists of four pairs of diode-bidirectional switch and two median diodes allowing the output voltage of the inverter to be at zero level. The center point of each arm is connected to a dc source.

To avoid short-circuits of the voltage sources by conduction, and in order to deliver the three levels of the desired voltages, then one must make the inverter work in its commendable mode. A static converter commendable mode means that the transitions between its various configurations depend only on external control and not on its internal control.

4.2. Modeling structure of one inverter arm

The structure symmetry of the three level inverter facilitates arm modeling, as shown in Fig. 2. One initially defines the global model of an arm, and then deduces that of the complete inverter.

Figure 2: Modeling structure of one inverter arm

Table 1: Switches excitation

G_{k1}	G_{k2}	G_{k3}	G_{k4}	V_{ko}
0	0	1	1	V_{c2}
0	1	0	1	unknown
1	0	1	0	0
1	1	0	0	V_{c1}

Three complementary controls can be applied to the three level inverter arm.

$$G_{k3} = \overline{G_{k1}} \qquad G_{k2} = \overline{G_{k1}} \qquad G_{k4} = \overline{G_{k1}}$$
$$G_{k4} = \overline{G_{k2}} \qquad G_{k4} = \overline{G_{k3}} \qquad G_{k3} = \overline{G_{k2}}$$

????With G_{ks} the trigger controls of the T_{ks} switch of the arm K.???? In order to have the total commendable mode of the three level inverter, one must eliminate the case which gives an unknown answer.

By translating this complementary control using the connection functions of the switches of arm K, one finds:

$$\begin{cases} F_{k3} = 1 - F_{k4} \\ F_{k2} = 1 - F_{k3} \end{cases} \tag{10}$$

One defines the connection function of the half-arms noted as F^b_{km} with:

$$m = \begin{cases} 1 \text{ for the higher half arm composed of } TD_{k1} \text{ and } TD_{k2} \\ 0 \text{ for the lower half arm composed of } TD_{k3} \text{ and } TD_{k4} \end{cases}$$

The connection functions of the half-arms are expressed by means of the connection functions of the switches as follows:

$$\begin{cases} F^b_{k1} = F_{k1}F_{k2} \\ F^0_{k1} = F_{k3}F_{k4} \end{cases} \tag{11}$$

The nodal potentials a, b, c of the three phase three level inverter compared to the medium point, are given by the following system:

$$\begin{cases} v_{ao} = F_{11}F_{12}v_{c1} - F_{13}F_{14}v_{c2} \\ v_{bo} = F_{21}F_{22}v_{c1} - F_{23}F_{24}v_{c2} \\ v_{co} = F_{31}F_{32}v_{c1} - F_{33}F_{34}v_{c2} \end{cases} \tag{12}$$

By introducing the connection functions of the half arms, one

will obtain:

$$\begin{cases} v_{ao} = F^b_{11}v_{c1} - F^b_{10}v_{c2} \\ v_{bo} = F^b_{21}v_{c1} - F^b_{20}v_{c2} \\ v_{co} = F^b_{31}v_{c1} - F^b_{30}v_{c2} \end{cases} \tag{13}$$

The inverter output phase voltages are deduced in terms of the nodal potentials compared to the medium point by the following relation:

$$\begin{cases} v_a = \frac{1}{3}(2v_{ao} - v_{bo} - v_{co}) \\ v_b = \frac{1}{3}(-v_{ao} + 2v_{bo} - v_{co}) \\ v_c = \frac{1}{3}(-v_{ao} - v_{bo} + 2v_{co}) \end{cases} \tag{14}$$

From the relation (13) and (14), one obtains the matrix system linking the functions of the inverter half-arms to the phase voltages at the load terminals given as:

$$\begin{bmatrix} v_a \\ v_b \\ v_c \end{bmatrix} = \frac{1}{3}\begin{bmatrix} 2 & -1 & -1 \\ -1 & 2 & -1 \\ -1 & -1 & 2 \end{bmatrix}\begin{bmatrix} F^b_{11} \\ F^b_{21} \\ F^b_{31} \end{bmatrix}v_{c1} - \begin{bmatrix} F^b_{10} \\ F^b_{20} \\ F^b_{30} \end{bmatrix}v_{c2} \quad 4.6)$$

In the case where $v_{c1} = v_{c2} = \frac{v_f}{2}$, the relation (??) is reduced to:

$$\begin{bmatrix} v_a \\ v_b \\ v_c \end{bmatrix} = \frac{1}{3}\begin{bmatrix} 2 & -1 & -1 \\ -1 & 2 & -1 \\ -1 & -1 & 2 \end{bmatrix}\begin{bmatrix} F^b_{11} - F^b_{10} \\ F^b_{21} - F^b_{20} \\ F^b_{31} - F^b_{30} \end{bmatrix}\frac{v_f}{2} \tag{15}$$

5. Three level inverter control strategy

5.1. Principle of triangular-sinusoidal control:

To determine in real time the instants of switches closing and opening, one makes use of analogical or numerical control. The pulse width modulation (PWM) allows us to achieve this objective. Its principle consists in using the intersections of a reference wave (the output wave image of what one wants to obtain) generally sinusoidal, with a modulation wave (known as the carrying wave) that is generally triangular.

5.2. Triangular-sinusoidal (SPWM) Characteristics

If the reference wave is sinusoidal, two parameters characterize the control:

- The index of modulation (m): defined by the ratio of the carrying and reference wave frequencies fp/fr.

- The modulation factor (r): defined by the ratio of the amplitudes of the reference and carrying voltages V_{rm}/V_{pm}, (also called the amplitudes ratio).

To have the maximum points of intersection between the two signals (carrying and reference), the modulation factor must be lower than $1(r < 1)$; when r is higher than $1(r > 1)$, we obtain an over modulation, which means the disappearance of certain intersections between the sinusoidal and triangular waves.

5.3. Space Vector PWM for Three level Inverters [10, 11]

The space vector concept, which was originally derived from the rotating field of induction motors, is used in the application of pulse width modulation. Space vector PWM (SVPWM) is a more sophisticated technique for generating modulation signals, and it has many advantages over conventional SPWM techniques:

- reduced commutation losses,

- higher amplitude of the modulation index,

- greater DC-bus voltage utilization, and

- lower total harmonic distortion (THD) of the output voltages.

The above advantages have allowed this novel technique to be increasingly used in industry over the last decade [12]. Unlike other methods, Vector PWM is not based on separate calculations for each of the modulations of the inverter arm. In this modulation the desired three sinusoidal output voltages are represented by a single vector. This vector is best approximated for each modulation interval by acting on the control of the three sets of complementary switches. SVPWM is not based on separate calculations for each arm of the inverter, but the determination of a global control vector approximated in an over modulation T.

5.4. SVPWM characteristics in a three level inverter:

V_{io} is related to the E voltage through ($i = a$, b, c):

$$V_{io} = C_i \frac{E}{2} \tag{16}$$

The simple voltage Vin between the phase and the neutral point depends on V_{io} via:

$$V_{in} = V_{io} - V_{no} \tag{17}$$

Assuming that the system is balanced, the sum of V_{in} ($i = a$, b, c) is equal to zero:

$$V_{an} + V_{bn} + V_{cn} = 0 \tag{18}$$

By the expressions (16), (17) we find:

$$V_{no} = \frac{1}{3} (V_{ao} + V_{bo} + V_{co}) \tag{19}$$

Replacing (18) in (16) the following matrix is:

$$\begin{bmatrix} V_{an} \\ V_{bn} \\ V_{cn} \end{bmatrix} = \begin{bmatrix} \frac{2}{3} & \frac{-1}{3} & \frac{-1}{3} \\ \frac{-1}{3} & \frac{2}{3} & \frac{-1}{3} \\ \frac{-1}{3} & \frac{-1}{3} & \frac{2}{3} \end{bmatrix} \cdot \begin{bmatrix} V_{ao} \\ V_{bo} \\ V_{co} \end{bmatrix} \quad (5.5)$$

The Concordia transformation is applied to the Vin vector:

$$\begin{bmatrix} V_\alpha \\ V_\beta \end{bmatrix} = \sqrt{\frac{2}{3}} \begin{bmatrix} 1 & \frac{-1}{2} & \frac{-1}{2} \\ 0 & \sqrt{\frac{3}{2}} & -\sqrt{\frac{3}{2}} \end{bmatrix} \cdot \begin{bmatrix} V_{an} \\ V_{bn} \\ V_{cn} \end{bmatrix} \tag{20}$$

The variable can take the three states ($C = 1, 0, -1$), and with our three phase inverter the number of possible combinations is $3^3 = 27$ combinations or vectors.

Table 2: Space vectors voltages

| Zero Voltages	Small Voltages	Medium Voltages	Full Voltages
V_0 (0,0,0)	V_1 (1,0,0)	V_{21} (1,0,-1)	V_{15} (1,-1,-1)
	V_8 (0,-1,-1)		
	V_2 (1,1,0)	V_{22} (0,1,-1)	V_{16} (1,1,-1)
	V_9 (0,0,-1)		
V_7 (1,1,1)	V_3 (0,1,0)	V_{23} (-1,1,0)	V_{17} (-1,1,-1)
	V_{10} (-1,0,-1)		
	V_4 (0,1,1)	V_{24} (-1,0,1)	V_{18} (-1,1,1)
	V_{11} (-1,0,0)		
V_{14} (-1,-1,1)	V_5 (0,0,1)	V_{25} (0,-1,1)	V_{19} (-1,-1,1)
	V_{12} (-1,-1,0)		
	V_6 (1,0,1)	V_{26} (1,-1,0)	V_{20} (1,-1,1)
	V_{13} (0,-1,0)		

Figure 3: Three phase voltage space vectors in the $\alpha\beta$ plane

Figure (3) shows the representation of 27 voltage vectors for the three level inverter.

Depending on the size of the voltage, vectors are divided into four groups, as represented in Table 2:

6. Simulation results

The power system described above was simulated by MATLAB/Simulink, as is shown in Fig. 5.

The stator of the machine is connected directly to a three phase grid, the rotor is powered by a three phase, three level inverter controlled primarily by SPWM, and then by SVPWM. The parameters of the DFIG are given in the appendix. A random wind profile (Fig. 5) is applied to the system. Fig. 7 shows the time trend of the mechanical speed of the turbine. From the curves of electromagnetic torque (Fig. 8 and 9), a difference can be seen. Indeed, torque obtained with the SVPWM command of the inverter is much better than the SPWM technique (oscillations in this case are more significant and this is caused by the fact that direct stator currents ids and quadrature iqs, which are represented respectively in Fig. 10 and 12, show less oscillation in the SVPWM relative to the SPWM.
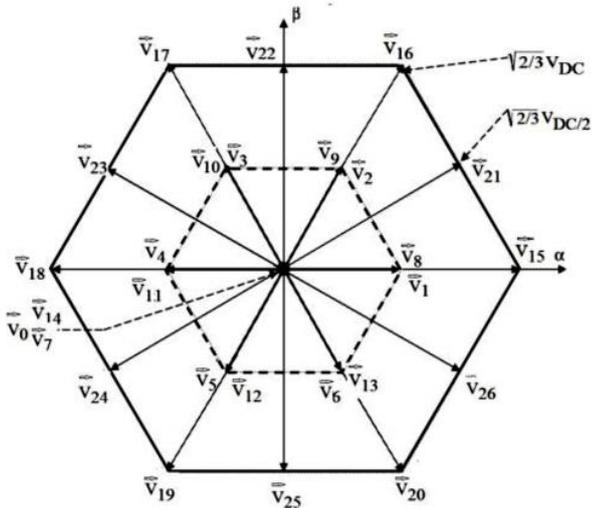
Figure 4: Three level inverter hexagons [13]

In Fig. 13, the three phase system of stator currents wave forms are closer to the suitable sinusoidal signal, However, the ripples in powers are more significant in the SPWM strategy. The same report is felt in the stator active and reactive power.

To achieve a fair comparison, we used the Fast Fourier Transform (FFT) algorithm; it is commonly used in digital signal processing to transform discrete time domain data to the frequency domain.

Fig. 19 shows the waveforms and the harmonic spectra of the voltage obtained at the output of the three level inverter for the two strategies (a: SPWM, b: SVPWM).

The results between the two (SPWM- SVPWM) control strategies are compared and summarized in Table 3.

The simulation and the analysis of the curves deliver very similar results for both control techniques, with a slight advantage for the control system with vector PWM.

This is verified by the FFT analysis results, where it can be seen that the Total Harmonic Distortions (THD) of the SVPWM technique are reduced compared with SPWM for all parameters (inverter voltage, the stator currents is, and even for active and reactive power).

7. Conclusion

This paper deals with control of a wind producing energy system based on a DFIG.

The rotor voltage is generated by a three phase, three level inverter with NPC structure. A comparative study of two control strategies is made; first SPWM then SVPWM.

Figure 5: Global structure of the power system

Table 3: THD Values for PWM and SVPWM

Settings	THD SPWM (%) command	THD SVPWM (%) command
Output inverter Voltage	66.05	42.63
stator current	0.66	0.65
Electromagnetic torque	4.30	0.96
Current isd	37.02	34.99
Current isq	21.42	14.80
Active power	20.50	15.11
Reactive power	36.99	34.52

The modeling of the inverter and the DFIG has been detailed. The comparative study addresses two control strategies, which are slightly different for the two types of control. It is verified by the FFT analysis

The THD spectra showed that SVPWM offers a better choice. The system studied in this paper is part of a complete system that can be of interest in a wind power generation system. Future experimental works will validate our simulation results.

References

[1] The World Wind Energy Assosiation report on Wind Energy available online at http://www.wwindea.org.

[2] B. Wu, Y. Lang, N. Zargari, S. Kouro, Power conversion and control of wind energy systems, John Wiley & Sons, 2011.

[3] F. Poitiers, T. Bouaouiche, M. Machmoum, Advanced control of a doubly-fed induction generator for wind energy conversion, Electric Power Systems Research 79 (7) (2009) 1085–1096.

[4] B.Multon, X.Roboam, B.Dakyo, C.Nichita, O.Gergaud, H.BenAhmed,"Aérogénérateurs électriques". Technique De L'ingénieur, D 3 960, 2008.

[5] M. Manjrekar, G. Venkataramanan, Advanced topologies and modulation strategies for multilevel inverters, in: Power Electronics Specialists
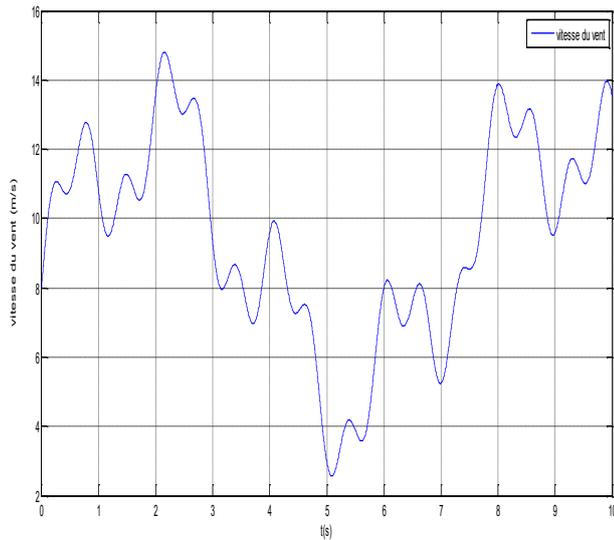
Figure 6: Wind speed
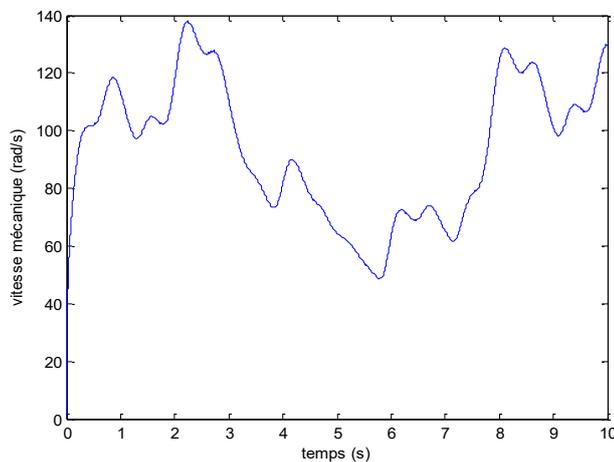
Figure 7: Turbine mechanical speed
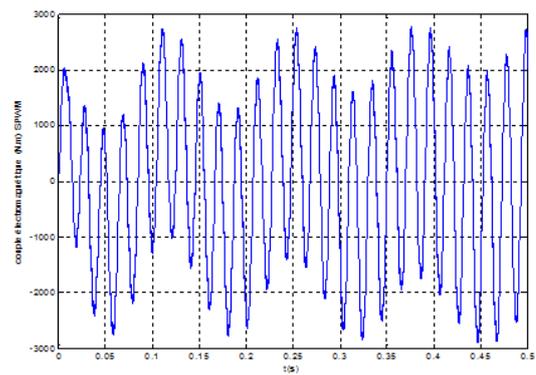
Figure 8: Electromagnetic torque—SPWM
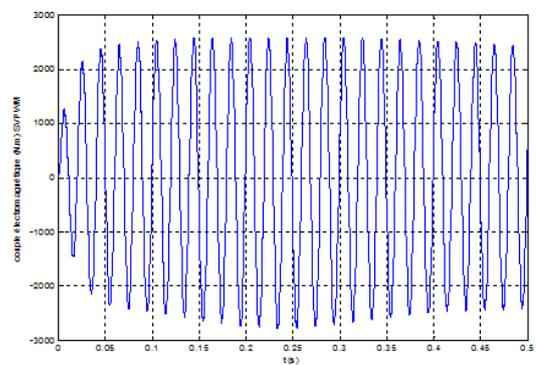
Figure 9: Electromagnetic torque—SVPWM

Conference, 1996. PESC'96 Record., 27th Annual IEEE, Vol. 2, IEEE, 1996, pp. 1013–1018.

[6] F. Blaabjerg, Z. Chen, S. B. Kjaer, Power electronics as efficient interface in dispersed power generation systems, IEEE transactions on power electronics 19 (5) (2004) 1184–1194.

[7] M. Kadjoudj, F. Louai, A. Benoudjit, C. Ghennai, Simulation of two and three level vsi induction motor drive, in: The 1997 32 nd Univertsities Power Engineering Conference, UPEC'97. Part 2(of 2), 1997, pp. 1018–1021.

[8] J. A. Baroudi, V. Dinavahi, A. M. Knight, A review of power converter topologies for wind generators, Renewable Energy 32 (14) (2007) 2369–2385.

[9] H. Camblong, G. Tapia, M. Rodriguez, Robust digital control of a wind turbine for rated-speed and variable-power operation regime, IEE Proceedings-Control Theory and Applications 153 (1) (2006) 81–91.

[10] F. Poitiers, Etude et commande de generatrices asynchrones pour l'utilisation de l'energie eolienne-machine asynchrone à cage autonome-machine asynchrone à double alimentation reliée au réseau, Ph.D. thesis, Université de Nantes (2003).

[11] S. El Aimani, Modélisation des différentes technologies d'éoliennes intégrées dans un réseau de moyenne tension, Ph.D. thesis, Ecole Centrale de Lille (2003).

[12] K. Lavanya, V. Rangavalli, A novel technique for simulation & analysis of svpwm two &three level inverters, International Journal of Engineering Research and Application 3 (2013) 455–460.

[13] C. Bächle, H. Bauer, T. Seger, Requirements on the control of a three-level four quadrant power converter in a traction application, in: 3rd European Conference on Power Electronics and Applications (EPE),(Aachen, Federal Republic of Germany), 1989, pp. 577–582.

[14] L. Hu, H. Wang, Y. Deng, X. He, A simple svpwm algorithm for multi-level inverters, in: Power electronics specialists conference, 2004, pp. 3476–3480.
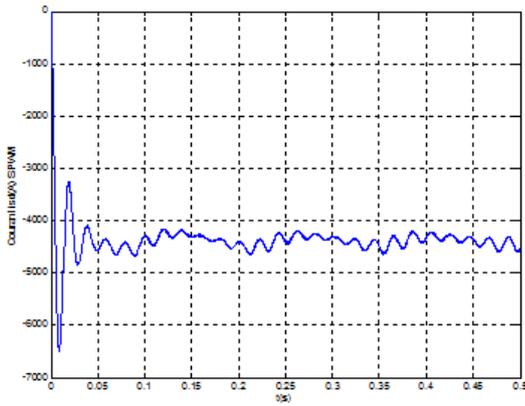
Figure 10: Stator current isd—SPWM

Figure 11: Stator current isd—SVPWM

Figure 12: Stator current isq—SPWM
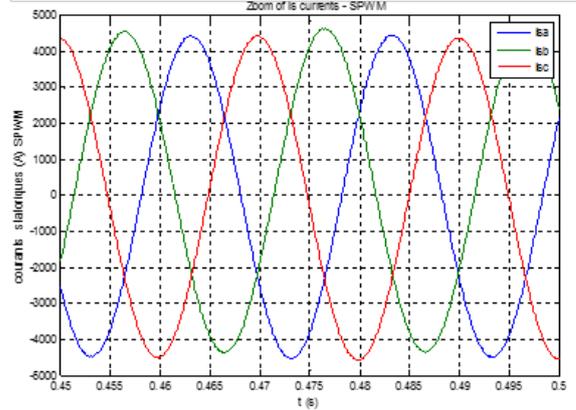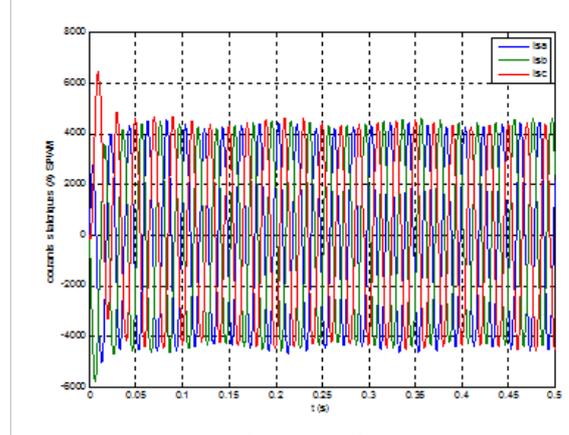

Figure 13: Stator currents is—SPWM
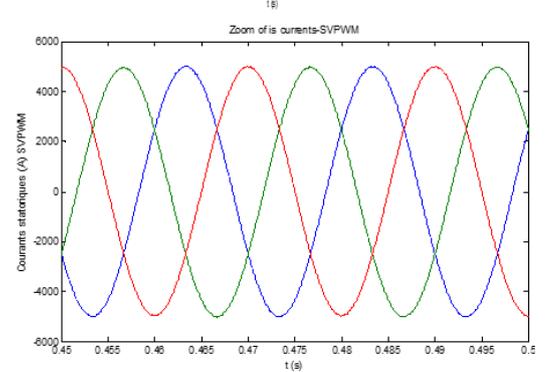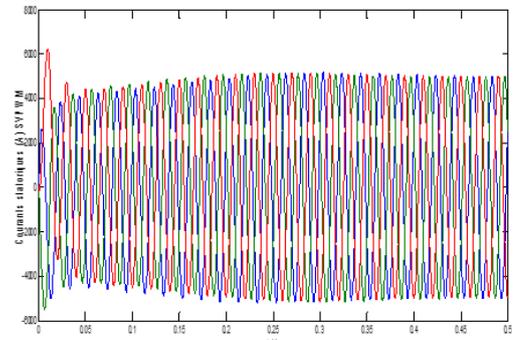

Figure 14: Stator currents is—SVPWM
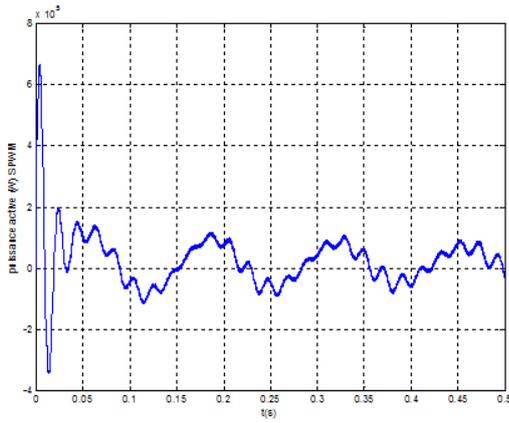
Figure 15: Active power—SPWM
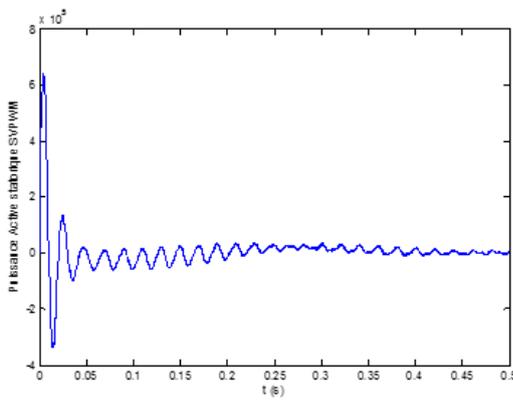

Figure 16: Active power—SVPWM
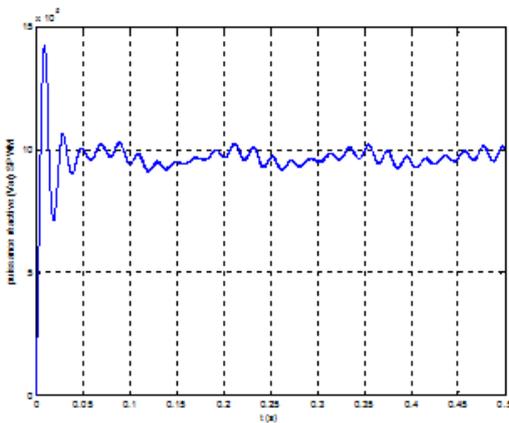
Figure 17: Reactive power—SPWM
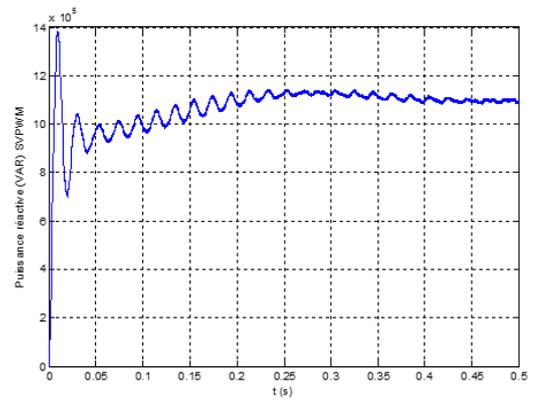
Figure 18: Reactive power—SVPWM
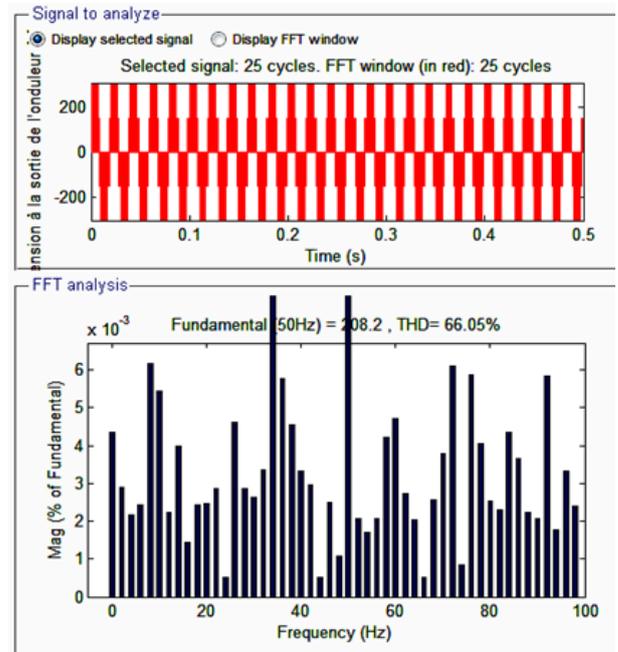
Figure 19: Harmonic spectrum of output inverter Voltage SPWM

Wind turbine parameters [14]	
Blade length , R , m	35.25
Number of blades	3
Air density, kg/m^3	1.225
Viscous friction coefficient, f, Nm/s	0.0024
Gearbox ratio, G	90
DFIG parameters	
Moment of inertia, J, kg/m^2	1000
Stator rated voltage, Vs, v	398/690
Stator rated frequency, f, Hz	50
Stator resistance, Rs, Ω	0.012
Rotor resistance, Rr, Ω	0.021
Stator inductance, Ls, H	0.0137
Rotor inductance, Lr, H	0.0136
Mutual inductance, Lm, H	0.0135
Number of pair of poles, p	2
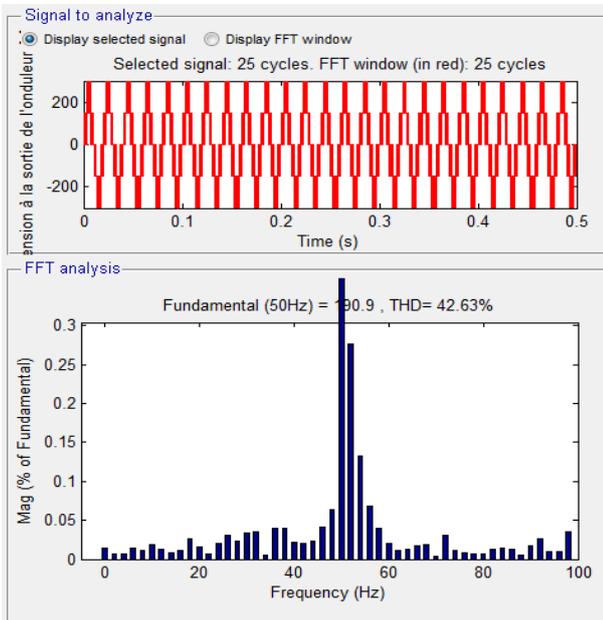
Figure 20: Harmonic spectrum of output inverter Voltage SVPWM
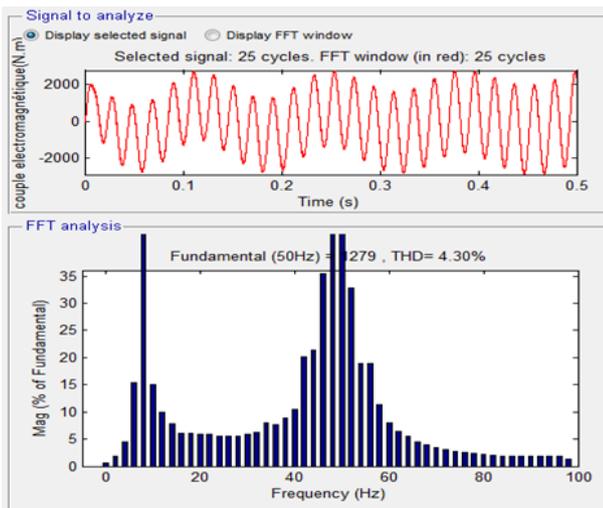
Figure 21: Harmonic spectrum of electromagnetic torque
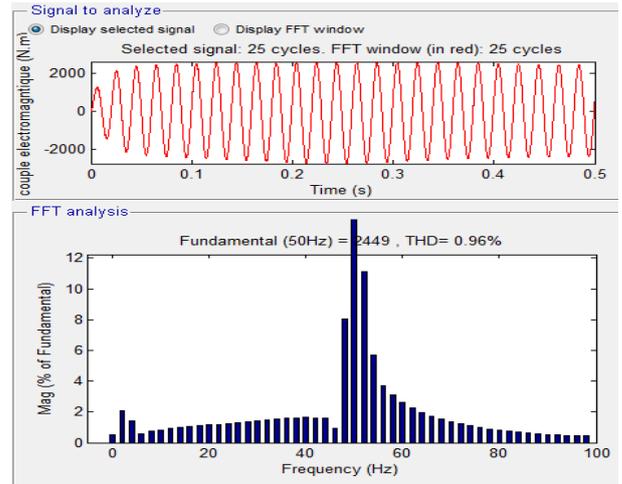
Figure 22: Harmonic spectrum of electromagnetic torque SVPWM
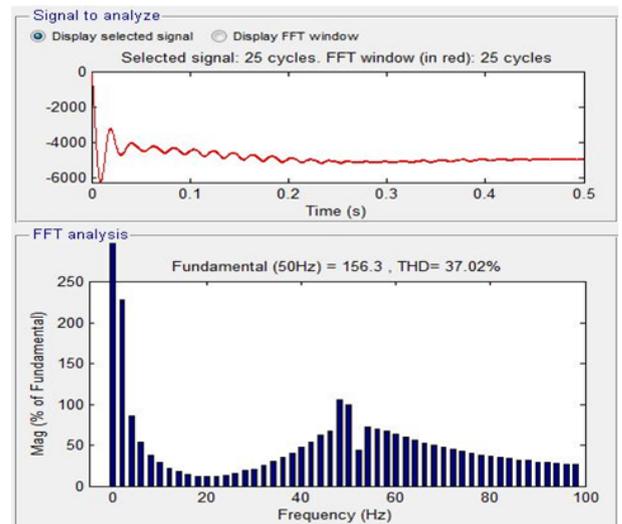
Figure 23: Harmonic spectrum of isd current SPWM
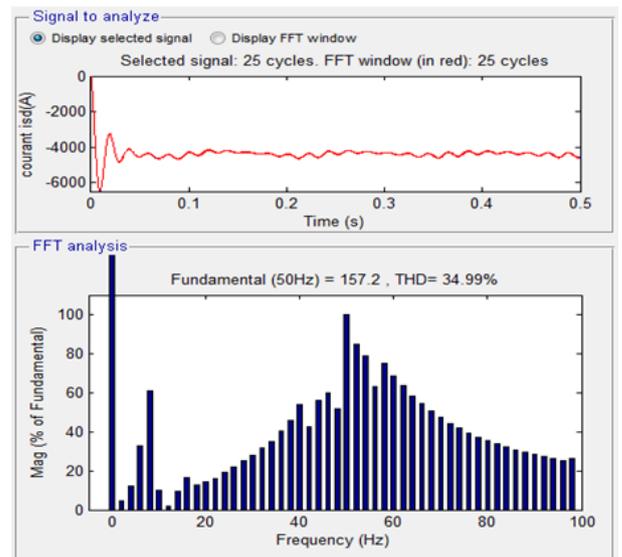
Figure 24: Harmonic spectrum of isd current SVPWM
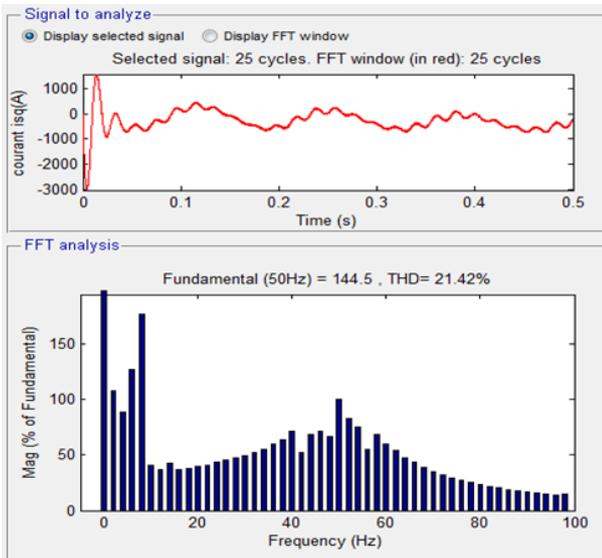
Figure 25: Harmonic spectrum of isq current SPWM
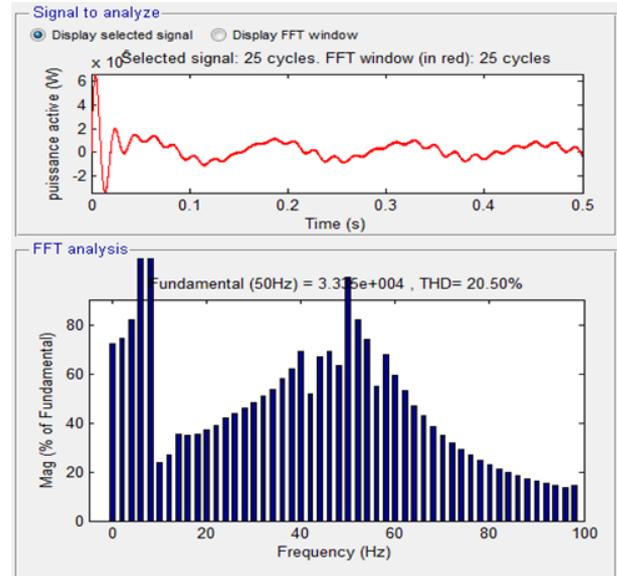
Figure 27: Harmonic spectrum of active power SPWM
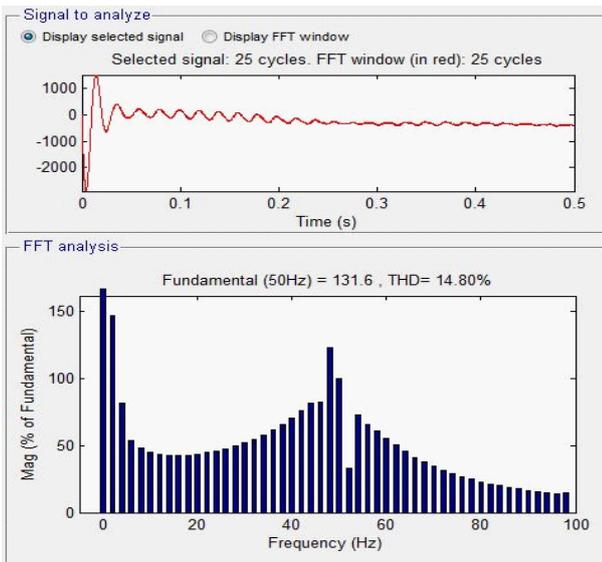
Figure 26: Harmonic spectrum of isq current SVPWM
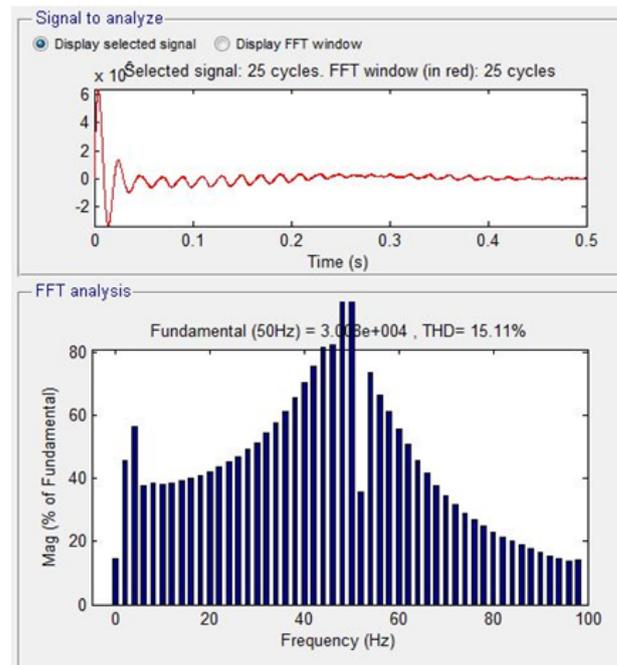
Figure 28: Harmonic spectrum of active power SVPWM
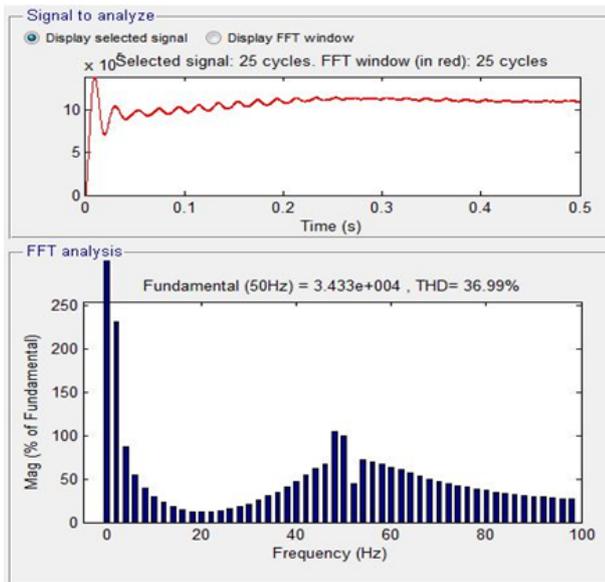
Figure 29: Harmonic spectrum of reactive power SPWM
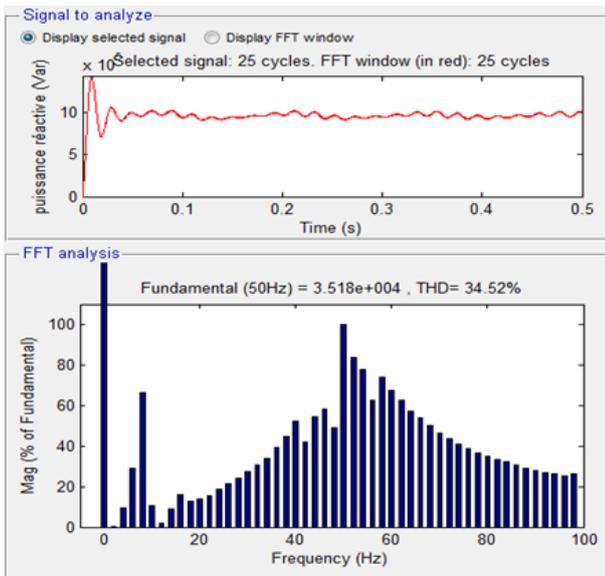
Figure 30: Harmonic spectrum of reactive power SVPWM